

Modelling, Analysis and Control of OmniMorph: an Omnidirectional Morphing Multi-rotor UAV

Youssef Aboudorra¹, Chiara Gabellieri¹, Quentin Sablé¹, Antonio Franchi^{1,2,3}

Abstract—We present the design, modelling, and control of a novel morphing multi-rotor Unmanned Aerial Vehicle (UAV) that we call the OmniMorph. The morphing ability allows the platform to switch between different configurations to achieve the required task. The *uni-directional thrust* (UDT) configuration can be used for energy-efficient navigation, while *fully-actuated* (FA) and *omni-directional* (OD) configurations can be used for full pose tracking and make the platform assume any orientation while compensating the gravity. The platform is equipped with eight bi-directional propellers that are actively tilted in a synchronized fashion using only one additional degree of actuation.

I. INTRODUCTION

Over the last decade design, perception, and control of aerial robotics evolved substantially when it comes to the functionalities and capabilities of Unmanned Aerial Vehicles (UAVs) indoors or outdoors. Research now considers the use of UAVs as Aerial Robotic Manipulators that can interact physically with the environment [1] and humans [2], where contact-based inspection [3], object manipulation [4], and assisting human workers [5] are some of the typical tasks. This led to the development of multi-rotor aerial vehicles (MRAVs) and the exploration of new designs different from the popular underactuated multirotor design that uses fixed coplanar/collinear propellers (i.e., quadrotors, hexarotors, and their variants). The new designs are based on choosing the number, position, and orientation of the propellers to provide the multirotor with different actuation properties and abilities to achieve a specific task [6].

In [7], a novel metric to assess the omnidirectional property of a generic multi-rotor aerial vehicle was presented. This metric is calculated numerically from the force set of the platform, and as such rely on the platform geometry and thrusters; moreover, it allows a direct assessment of a platform's omnidirectional property given its weight. [7] also showed the use of this metric in the process of upgrading the design presented in [8], by placing the propellers on a virtual sphere centered around the platform's center of mass (CoM) instead of the same plane with the platform's CoM.

¹Robotics and Mechatronics lab, Faculty of Electrical Engineering, Mathematics & Computer Science, University of Twente, Enschede, The Netherlands y.a.l.a.aboudorra@utwente.nl, c.gabellieri@utwente.nl, a.franchi@utwente.nl

²Department of Computer, Control and Management Engineering, Sapienza University of Rome, 00185 Rome, Italy antonio.franchi@uniroma1.it

³LAAS-CNRS, Université de Toulouse, CNRS, 31400 Toulouse, France antonio.franchi@laas.fr

This work was partially funded by European Commission project H2020 AERIAL-CORE (871479) and MSCA project Flyfic (101059875)

Recently, several works addressed the design of omnidirectional multirotors and presented working prototypes. Each of those designs relied on a different actuation strategy to achieve omnidirectional flight. We categorize them into three main types.

The first type uses fixedly tilted *bi-directional* propellers (which generate thrust on both sides of the spinning direction, by inverting the sense of rotation). The authors in [9] presented one of the first omnidirectional prototypes, where they placed eight bi-directional propellers on the edges of a cube. The novelty of their design is the optimization-based placement and orientation of the propellers, where the cube shape was chosen to ensure a rotation-invariant inertia tensor. Another omnidirectional design with fixed propellers was presented in [10] and [11], achieving omnidirectional wrench generation with six and eight bi-directional propellers, respectively.

The second type, like the design proposed in [12], optimizes the orientation of fixed *uni-directional* propellers (i.e., able to produce thrust on only one side of the spinning direction, or in other words, to rotate in only one sense) to achieve omnidirectionality while balancing the lift among the different propellers and aiming for a sphere-like shape of the corresponding force set. In fact, [12] showed that the minimal number of 7 (seven) uni-directional propellers is necessary to achieve omnidirectional position and orientation tracking. Later, [8] presented a working prototype of the design with experiments.

The third type relies on a morphing design. It uses uni- or bi-directional propellers which are *actively tilted* by servo motors. [13] propose a quadrotor with propellers individually tilting about their radial axis. The authors of [14] presented an omnidirectional platform, consisting of a hexarotor design with each propeller rotating about its radial axis. Another version of their design was presented in [15], in which double propeller groups were used, two propellers rotating in opposite directions on each rotation axis to increase the platform efficiency, payload capacity, in addition to increased force bounds along different directions.

The advantage of the third design approach relies on the possibility to optimize the energy consumed for a given desired orientation, which is obtained by aligning as much as possible the propeller spinning directions for a given orientation. This also allows balancing dexterity and energy efficiency based on the needs imposed by specific tasks [16] [17]. Indeed, the configuration in which all the directions are aligned is more energetically efficient. In that configuration, the propeller forces are all parallel to each other while in the

other configurations there are propeller forces that cancel each other without actively contributing to the motion. This configuration is however not always possible. This is the price paid to achieve multi/omni-directionality.

Fixed-propeller multirotors in [9], [10], [8] can be controlled by (pseudo)inverting the wrench map between the propellers' speeds and the total body wrench. The system is affine in the control inputs and the tilting angles of the propellers are constant design parameters. A similar control approach is used in [11], where a different rotor input allocation is proposed, based on the infinity-norm minimization; in this way, propellers' speed constraints are implicitly taken into account. To control the third type of omnidirectional platforms, feedback linearization at the jerk level has been proposed [13]. With the time-differentiation, the system is affine in the (new) control inputs, but the control law requires the full allocation matrix to be non-singular.

In this work, we overcome some of the limitations of existing designs and controls of omnidirectional platforms. Specifically, the contributions of this work are as follows.

- A novel omnidirectional platform design concept, the OmniMorph, is proposed. The platform belongs to the third type described in this section and exploits the synchronized drive of all propellers by only one servo motor, so to keep at the bare minimum the additional payload used to host additional servo motors.
- The actuation properties of the OmniMorph are formally studied.
- A novel control method is proposed for multi-rotors with actively and synchronously tilting propellers. Compared to the state of the art, the proposed controller allows automatic transitions between underactuated and omnidirectional configurations; furthermore, it accounts for input constraints, only indirectly handled through redundancy resolution in the literature [13].
- The proposed design and controller are tested in a realistic simulation environment.

II. OMNIMORPH DESIGN AND MODEL

A. Concept and Design

The OmniMorph platform consists of 8 bi-directional propellers attached to the main body frame, placed on the vertices of a cube centered at the CoM. Each propeller can tilt around an axis that lies along the edge of the cube. All propellers tilt in a synchronized way as all are attached to a single extra actuation unit (tilting mechanism) driven by only one servo motor. Hence, all propellers always have the same angle around the respective rotation axes. The concept of synchronized tilting has been previously used in a fully-actuated but not omnidirectional platform in [16], [17]. The change in the orientation of the propellers (morphing), enables the platform to switch between different actuation capabilities. When all rotors are parallel to each other (i.e. tilting angle α equal to zero) the generated thrust can be only produced along one axis, making the vehicle underactuated (UA)—see Figure 1 left. In this case, the platform is,



Fig. 1: The OmniMorph: UA configuration (left) and OD configuration (right).

from the actuation point of view, equivalent to the standard underactuated quadrotor, hexarotor, and so on: only 4 DoFs are independently controlled, the 3D position and the heading angle. This configuration is the most energetically efficient and it is recommended in tasks in which the control of the full orientation or full wrench is not essential.

As the tilting angle α of the propeller deviates from zero, the total thrust can be generated in all three orthogonal directions, to a certain extent, depending on the tilting configuration. Ultimately, the vehicle can assume an OD configuration similar to the vehicle developed in [9]—see Figure 1, right. Such a configuration allows controlling the 6D full pose of the vehicle.

B. Model of the OmniMorph

We define an inertial frame as a set of an origin and three orthogonal axes: $\mathcal{F}_W : \{O_W, \mathbf{x}_W, \mathbf{y}_W, \mathbf{z}_W\}$. Similarly, we define a reference frame attached to the robot, $\mathcal{F}_B : \{O_B, \mathbf{x}_B, \mathbf{y}_B, \mathbf{z}_B\}$ where the origin, O_B , is coincident with the robot Center of Mass (CoM). The position of O_B in \mathcal{F}_W is indicated as \mathbf{p} and its attitude is expressed compactly as $\mathbf{R} := {}^W \mathbf{R}_B$.¹

Also, we define a frame attached to each propeller $\mathcal{F}_{p_i} : \{O_{p_i}, \mathbf{x}_i, \mathbf{y}_i, \mathbf{z}_i\}$. The origin O_{p_i} corresponds to the center of the i -th propeller. The vector between O_B and O_{p_i} is \mathbf{p}_{p_i} . The axis \mathbf{z}_i is chosen parallel to the line about which the brushless motor and the propeller rotate, called the spinning axis of the i -th propeller. The axis \mathbf{y}_i is chosen perpendicular to both \mathbf{z}_i and \mathbf{p}_{p_i} . The remaining axis is $\mathbf{x}_i = \mathbf{y}_i \times \mathbf{z}_i$.

The main quantities are defined in Table I. The dynamic equations of the robot, expressed as Newton-Euler equations of an actuated rigid body, are as follows, where the translational dynamics is expressed in the inertial frame and the rotational dynamics in the body frame. We indicate as $\boldsymbol{\omega}$ the angular velocity of \mathcal{F}_B w.r.t \mathcal{F}_W expressed in \mathcal{F}_B , with m the robot mass, and with $\mathbf{J} \in \mathbb{R}^{3 \times 3}$ its rotational inertia.

$$\begin{bmatrix} m\mathbf{I}_3 & \mathbf{0}_3 \\ \mathbf{0}_3 & \mathbf{J} \end{bmatrix} \begin{bmatrix} \ddot{\mathbf{p}} \\ \dot{\boldsymbol{\omega}} \end{bmatrix} = \begin{bmatrix} -mge_3 \\ -\boldsymbol{\omega} \times \mathbf{J}\boldsymbol{\omega} \end{bmatrix} + \begin{bmatrix} \mathbf{R} & \mathbf{0}_3 \\ \mathbf{0}_3 & \mathbf{I}_3 \end{bmatrix} \begin{bmatrix} \mathbf{f}_B^B \\ \boldsymbol{\tau}_B^B \end{bmatrix} \quad (1)$$

¹In general, we indicate as ${}^A \mathbf{R}_{A'}$ the rotation from frame \mathcal{F}_A to $\mathcal{F}_{A'}$.

The rotational kinematics of the robot is:

$$\dot{\mathbf{R}} = \mathbf{R}[\boldsymbol{\omega}]_{\times}. \quad (2)$$

\mathbf{f}_B^B and $\boldsymbol{\tau}_B^B$ are the total force and torque applied to the CoM, expressed in \mathcal{F}_B .

Each rotor produces a thrust force and a drag moment which we model, similarly to [18], as follows.

$$\mathbf{f}_i = c_f w_i |w_i| \mathbf{z}_i, \quad \boldsymbol{\tau}_{d_i} = k_i c_\tau w_i |w_i| \mathbf{z}_i, \quad (3)$$

where $c_f, c_\tau > 0$ are the thrust and drag coefficient, respectively, and w_i is a scalar with a module equal to the norm of the propeller angular velocity and a sign defined such that $w_i > 0$ when the thrust produced by the propeller has the same direction of \mathbf{z}_i . The drag moment is always opposite to the angular velocity of the propeller; as a consequence, $k_i = -1$ for propellers with descending chord (i.e., producing thrust in the same direction of the angular velocity, also called ‘counterclockwise’) and $k_i = +1$ for propellers with ascending chord (i.e., producing thrust in the opposite direction of the angular velocity, also called ‘clockwise’).

The applied body forces and torques are the result of all actuation units (rotors) and their orientation:

$$\mathbf{f}_B^B = \sum_{i=1}^n \mathbf{f}_i^B = \sum_{i=1}^n {}^B \mathbf{R}_{p_i} \mathbf{e}_3 f_i \quad (4)$$

$$\begin{aligned} \boldsymbol{\tau}_B^B &= \sum_{i=1}^n \boldsymbol{\tau}_{f_i}^B + \boldsymbol{\tau}_{d_i}^B = \sum_{i=1}^n \mathbf{p}_{p_i}^B \times \mathbf{f}_i^B + k_i c_\tau^B \mathbf{f}_i^B \\ &= \sum_{i=1}^n ([\mathbf{p}_{p_i}^B]_{\times} + k_i c_\tau^B \mathbf{I}_3) {}^B \mathbf{R}_{p_i} \mathbf{e}_3 f_i \end{aligned} \quad (5)$$

where $c_f^\tau = c_\tau / c_f$. We indicated with \mathbf{f}_i^B the thrust force of the i -th propeller expressed in \mathcal{F}_B , and with $\boldsymbol{\tau}_{f_i}^B$ and $\boldsymbol{\tau}_{d_i}^B$ the torque produced by the same propeller’s thrust at the body CoM and the effect of the propeller’s drag torque at the body CoM, respectively.

Note that the orientation of each rotor w.r.t to the body frame consists of two parts; a fixed rotation and an elementary rotation around the x -axis due to the single morphing

Definition	Symbol
inertial (world) frame $\mathcal{F}_W : \{O_W, \mathbf{x}_W, \mathbf{y}_W, \mathbf{z}_W\}$	\mathcal{F}_W
UAV body fixed frame (CoM) $\mathcal{F}_B : \{O_B, \mathbf{x}_B, \mathbf{y}_B, \mathbf{z}_B\}$	\mathcal{F}_B
i th rotor (propeller) frame $\mathcal{F}_{p_i} : \{O_{p_i}, \mathbf{x}_i, \mathbf{y}_i, \mathbf{z}_i\}$	\mathcal{F}_{p_i}
position of O_B in \mathcal{F}_W	$\mathbf{p} = {}^W \mathbf{p}_B$
rotation between \mathcal{F}_B and \mathcal{F}_W	$\mathbf{R} = {}^W \mathbf{R}_B$
angular velocity of \mathcal{F}_B w.r.t \mathcal{F}_W expressed in \mathcal{F}_B	$\boldsymbol{\omega}$
position of O_{p_i} w.r.t O_B in \mathcal{F}_B	$\mathbf{p}_{p_i}^B$
rotation from \mathcal{F}_B to \mathcal{F}_{p_i}	${}^B \mathbf{R}_{p_i}$
mass of the UAV	m
inertia matrix of the UAV w.r.t to O_B expressed in \mathcal{F}_B	\mathbf{J}
gravity acceleration	g
i th vector of the canonical basis of \mathbb{R}^3 , $i = 1, 2, 3$	\mathbf{e}_i
identity matrix of order 3	$\mathbf{I}_3 \in \mathbb{R}^{3 \times 3}$

TABLE I: Symbols and definitions

angle α :

$${}^B \mathbf{R}_{p_i} = {}^B \mathbf{R}_{h_i} \mathbf{R}_x(\alpha) \quad (6)$$

We call \mathbf{u} the input of the system, consisting of the single morphing angle α and the rotor speeds contained in the vector \mathbf{u}_w such that

$$\mathbf{u}_w = [u_{w_1} \cdots u_{w_n}]^\top = [w_1 |w_1| \cdots w_n |w_n|]^\top \in \mathbb{R}^n. \quad (7)$$

Hence, one has $\mathbf{u} = [\mathbf{u}_w^\top \ \alpha]^\top \in \mathbb{R}^9$. Based on (4) and (5), we have that the body wrench is

$$\mathbf{w}(\mathbf{u}) = \begin{bmatrix} \mathbf{f}_B^B \\ \boldsymbol{\tau}_B^B \end{bmatrix} = \mathbf{A}(\alpha) \mathbf{u}_w, \quad (8)$$

where $\mathbf{A}(\alpha)$ is the so called *wrench map*.

C. Actuation Properties

First, we define the *full allocation matrix* $\mathbf{F}(\mathbf{u}) \in \mathbb{R}^{6 \times 9}$ as in [6]:

$$\mathbf{F}(\mathbf{u}) = [\mathbf{F}_1(\alpha) \ \mathbf{F}_2(\mathbf{u}_w, \alpha)] \quad (9)$$

with $\mathbf{F}_1(\alpha) = \frac{\partial \mathbf{w}}{\partial \mathbf{u}_w}(\alpha) \in \mathbb{R}^{6 \times 8}$, $\mathbf{F}_2(\mathbf{u}) = \frac{\partial \mathbf{w}}{\partial \alpha}(\mathbf{u}) \in \mathbb{R}^6$. Note that, for (8), $\mathbf{F}_1 = \mathbf{A}(\alpha)$ and $\mathbf{F}_2 = \frac{\partial(\mathbf{A}(\alpha) \mathbf{u}_w)}{\partial \alpha}$. Following the method provided in [6], we study the actuation properties of the platform by looking at the rank of $\mathbf{F}(\mathbf{u})$ in (9). When $\text{rank}(\mathbf{F}(\mathbf{u})) = 6$, the platform is fully actuated, possibly omnidirectional. Whenever $\text{rank}(\mathbf{F}(\mathbf{u})) < 6$, the platform is underactuated.

First, we note that the matrix is 6×9 , composed by $\mathbf{F}_2(\mathbf{u}) \in \mathbb{R}^{6 \times 1}$ and by $\mathbf{F}_1(\alpha) \in \mathbb{R}^{6 \times 8}$, which is the *static allocation matrix*, because it represents the allocation matrix if we keep the servo motor angle fixed. Studying the rank of the static allocation matrix, $\mathbf{F}_1(\alpha)$, helps us study the rank of the full allocation matrix, $\mathbf{F}(\mathbf{u})$. We can state the following:

- $\text{rank}(\mathbf{F}_1(\alpha)) = 4$ is a sufficient condition for the platform to be underactuated: the rank of the full allocation matrix $\mathbf{F}(\mathbf{u})$ can be at most $5 < 6$.
- $\text{rank}(\mathbf{F}_1(\alpha)) = 6$ is a sufficient condition for the system to be fully actuated;
- If $\text{rank}(\mathbf{F}_1(\alpha)) = 5$, the full-/under-actuation needs further analysis of $\mathbf{F}_2(\mathbf{u}) \in \mathbb{R}^{6 \times 1}$ in relation to $\mathbf{F}_1(\alpha)$.

We study the rank of $\mathbf{F}_1(\alpha)$ for various values of α :

$$\text{rank}(\mathbf{F}_1(\alpha)) = \begin{cases} 4 & \text{if } \alpha = 0 + k\pi, k \in \mathbb{N} \\ 5 & \text{if } \alpha = \frac{\pi}{2} \\ 6 & \text{otherwise} \end{cases} \quad (10)$$

So, from what has been said so far, the OmniMorph is underactuated for $\alpha = 0$. However, $\text{rank}(\mathbf{F}(\mathbf{u}_w, 0)) = 5$ if $\mathbf{u}_w \neq \mathbf{0}$ and that not all u_{w_i} are equal to each other, i.e., the total wrench can be instantaneously changed on a ‘reduced’ five-dimensional manifold.

For $\alpha = \pi/2$, the OmniMorph results fully actuated ($\text{rank}(\mathbf{F}(\mathbf{u}_w, \pi/2)) = 6$ provided that $\mathbf{u}_w \neq \mathbf{0}$). An intuitive interpretation is provided in the following. When $\alpha = \pi/2$, all propellers’ thrusts are on the same plane in \mathcal{F}_B . The yaw can be controlled as the individual thrusts generate a

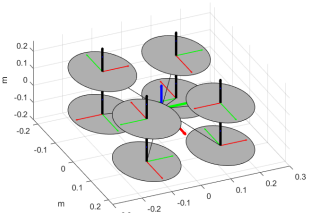
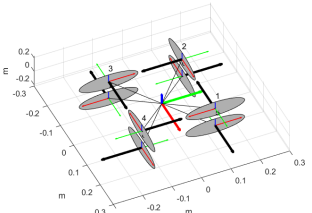
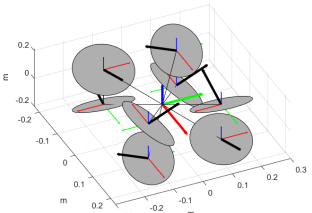
		
$\alpha = 0$	$\alpha = \frac{\pi}{2}$	$\alpha \neq \frac{\pi}{2}, \pi, 0$
Underactuated	Fully Actuated unless $\mathbf{u}_\omega = \mathbf{0}$	Fully Actuated, Redundant

TABLE II: Actuation properties for different values of α . Grey circles are the propellers' planes. Each is associated with a local frame, and a body-fixed frame is in the middle of the robot. The RGB convention is used to indicate the x-, y-, and z- axis, respectively. The direction of the thrust produced by the individual propellers is represented with a thick black arrow.

torque around the vertical axis of the robot. The pitch and roll are controlled thanks to the drag moment of the propellers. The position in the horizontal plane is clearly controlled by the thrust, but the position along \mathbf{z}_B is not. As soon as α changes, the propellers' thrusts have a component in the vertical direction as well, which gives controllability of the vertical position, unless the propellers' thrusts are actually zero (mathematically, $\mathbf{u}_w = \mathbf{0}$). In that case, $\text{rank}(\mathbf{F}(\mathbf{u})) = 5$ as $\mathbf{F}_2(\mathbf{u}, \alpha) = \mathbf{0}$. Please note that even if the platform is fully actuated it might not be able to fly properly because the propeller thrust intensity may be not large enough to sustain the platform's weight.

Eventually, for all other values of α , the platform is fully actuated. A schematic summary of the OmniMorph actuation properties is in Table II. For sufficiently large values of α , the polygon of the achievable forces contains a sphere whose radius corresponds to the weight of the platform: the robot can sustain its weight in any orientation.

The full allocation matrix is reported in the following for the sake of completeness:

$$\mathbb{F} = \frac{1}{c_f} \begin{bmatrix} -s_\alpha & 0 & s_\alpha & 0 \\ 0 & -s_\alpha & 0 & s_\alpha \\ c_\alpha & c_\alpha & c_\alpha & c_\alpha \\ Lc_\alpha - \frac{c_\tau s_\alpha}{c_f} & Lc_\alpha + Ls_\alpha & \frac{c_\tau s_\alpha}{c_f} - Lc_\alpha & -Lc_\alpha - Ls_\alpha \\ -Lc_\alpha - Ls_\alpha & Lc_\alpha + \frac{c_\tau s_\alpha}{c_f} & Lc_\alpha + Ls_\alpha & -Lc_\alpha - \frac{c_\tau s_\alpha}{c_f} \\ Ls_\alpha + \frac{c_\tau c_\alpha}{c_f} & Ls_\alpha - \frac{c_\tau c_\alpha}{c_f} & Ls_\alpha + \frac{c_\tau c_\alpha}{c_f} & Ls_\alpha - \frac{c_\tau c_\alpha}{c_f} \\ s_\alpha & 0 & -s_\alpha & 0 \\ 0 & s_\alpha & 0 & -s_\alpha \\ c_\alpha & c_\alpha & c_\alpha & c_\alpha \\ Lc_\alpha + \frac{c_\tau s_\alpha}{c_f} & Lc_\alpha + Ls_\alpha & -Lc_\alpha - \frac{c_\tau s_\alpha}{c_f} & -Lc_\alpha - Ls_\alpha \\ -Lc_\alpha - Ls_\alpha & Lc_\alpha - \frac{c_\tau s_\alpha}{c_f} & Lc_\alpha + Ls_\alpha & \frac{c_\tau s_\alpha}{c_f} - Lc_\alpha \\ \frac{c_\tau c_\alpha}{c_f} - Ls_\alpha & -Ls_\alpha - \frac{c_\tau c_\alpha}{c_f} & \frac{c_\tau c_\alpha}{c_f} - Ls_\alpha & -Ls_\alpha - \frac{c_\tau c_\alpha}{c_f} \end{bmatrix} \frac{\partial \mathbf{w}}{\partial \alpha}$$

D. Power Consumption Analysis

To analyze the power consumption of the OmniMorph, let us compute the input needed to enforce the static equilibrium when the platform is hovering with orientation $\mathbf{R} = \mathbf{I}_3$, this can be done by inverting (8) as

$$\mathbf{u}_w^h(\alpha, m) = (\mathbf{A}(\alpha))^\dagger \begin{bmatrix} mge_3 \\ \mathbf{0} \end{bmatrix}. \quad (11)$$

The power consumed by each brushless motor is equal to the scalar product between the motor torque and its

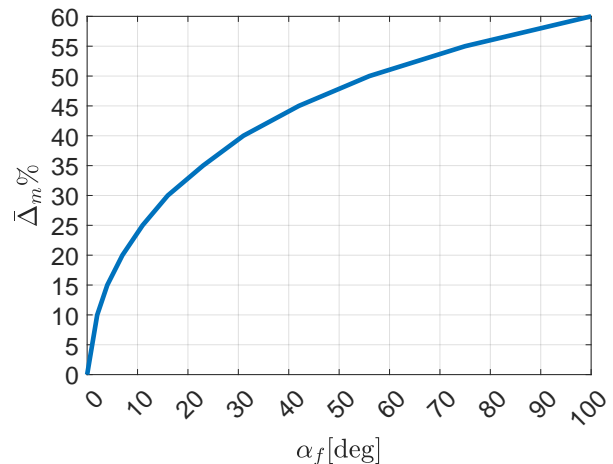


Fig. 2: For a given fixed propeller tilting angle α_f , a morphing design is convenient provided that the relative mass of the tilting mechanism is lower than $\bar{\Delta}_m$

angular velocity. Given that in hovering we can approximate the motor torque with the drag moment and that the drag moment is always opposing the angular velocity, we can write the power consumed by the i -th brushless motor as $P(u_{w_i}) = \|\boldsymbol{\tau}_{d_i}\| |w_i| = c_\tau |w_i|^3 = c_\tau |u_{w_i}|^{3/2}$. The total power consumed by all the motors is then

$$P_{\text{tot}}(\mathbf{u}_w) = \sum_{i=1}^8 P(u_{w_i}) = c_\tau \sum_{i=1}^8 |u_{w_i}|^{3/2}. \quad (12)$$

Therefore, $P_{\text{tot}}(\mathbf{u}_w^h(\alpha, m))$ represents the power consumed at hovering by a platform with a certain mass m and a given tilting angle α .

Let us now write the robot's mass as follows: $m = m_0(1 + \Delta_m)$, where Δ_m is the ratio between the mass of the propeller tilting mechanism and m_0 , which is the mass of all other components. Consider a multirotor in which a certain level of dexterity is obtained by tilting the propellers by a fixed angle α_f . We ask ourselves which is the critical relative mass of a tilting mechanism, $\bar{\Delta}_m$, below which a morphing design is convenient for such a platform, taking into account that the morphing design can hover with $\alpha = 0$ but will have $\Delta_m > 0$. To answer this question, we compute

numerically $\Delta_m(\alpha)$ as the solution of the following implicit relation between Δ_m and α

$$P_{\text{tot}}(\mathbf{u}_w^h(0, m_0(1 + \bar{\Delta}_m))) = P_{\text{tot}}(\mathbf{u}_w^h(\alpha_f, m_0)).$$

The values of $\bar{\Delta}_m$ as a function of α_f for the OmniMorph are reported in Figure 2. Clearly, for $\alpha_f = 0$, namely when no dexterity is required from the fixed-propeller platform, which is then a standard uni-directional platform, one has that $\bar{\Delta}_m = 0$. On the other side already for a needed α of 10 deg then the use of a morphing platform is more power efficient even for a weight of the tilting mechanism that constitutes up to 25% of all the other components. Omnidirectionality requires approximately $\alpha \geq 30\text{deg}$, which tells us that a morphing platform is more power efficient than a non-morphing one even for a weight of the tilting mechanism that constitutes up to 40% of all the other components'. Note that the minimum α to attain omnidirectionality depends on the maximum motor speed, on the propeller type, and the mass of the vehicle. We are considering here the same bi-directional propellers as in [19] with the same maximum motor speed and a mass $m_0 = 1.128\text{kg}$ equal to the mass of the OmniMorph without any tilting mechanism.

III. CONTROL

This section introduces a control law that allows the gf OmniMorph to follow a desired 6D trajectory switching between the underactuated and the fully actuated configurations to account for the minimization of trajectory tracking error and the minimization of the input \mathbf{u}_w .

Let us define $\ddot{\mathbf{q}} = [\ddot{\mathbf{p}}^\top, \dot{\boldsymbol{\omega}}^\top]^\top$. Given a reference trajectory for the UAV, indicated through the superscript $(\cdot)^d$, we compute the reference acceleration of the robot, call it $\ddot{\mathbf{q}}^r$, using a PD feedback control plus a feedforward term. The following desired input acceleration is obtained:

$$\ddot{\mathbf{q}}^r = \begin{bmatrix} \ddot{\mathbf{p}}^d + \mathbf{K}_{p1}\dot{e}_p + \mathbf{K}_{p2}e_p \\ \dot{\boldsymbol{\omega}}^d + \mathbf{K}_{\omega 1}e_\omega + \mathbf{K}_{\omega 2}e_R, \end{bmatrix} \quad (13)$$

where $e_R = \frac{1}{2}[\mathbf{R}^\top \mathbf{R}^d - \mathbf{R}^d \mathbf{R}]_\vee$, with \vee from $so(3)$ to \mathbb{R}^3 being the inverse of the hat map [20], $e_p = \mathbf{p}^d - \mathbf{p}$, and $e_\omega = \boldsymbol{\omega}^d - \boldsymbol{\omega}$.

We now design an inner control loop to track $\ddot{\mathbf{q}}^r$ thanks to suitable inputs α^* and \mathbf{u}_w^* , chosen as the solution to:

$$\begin{aligned} \min_{\alpha, \mathbf{u}_w, \ddot{\mathbf{q}}} \quad & J_1 + J_2 + J_3 \\ \text{s.t.} \quad & \mathbf{M}\ddot{\mathbf{q}} = \boldsymbol{\mu} + \mathbf{J}_R \mathbf{F}(\alpha) \mathbf{u}_w, \\ & \mathbf{C} \mathbf{u}_w < \mathbf{b}, \\ & -\epsilon_\alpha \leq \alpha - \alpha_{k-1}^* \leq \epsilon_\alpha \end{aligned} \quad (14)$$

where the cost function is composed of three terms: $J_1 = \|\mathbf{u}_w\|_{\mathbf{W}_1}^2$ is to minimize the norm of the input, $J_2 = \|\ddot{\mathbf{q}}^r - \ddot{\mathbf{q}}\|_{\mathbf{W}_2}^2$ to ensure tracking of the desired trajectory, and $J_3 = \|\mathbf{u}_w - \mathbf{u}_{w,k-1}^*\|_{\mathbf{W}_3}^2$ to minimize the propeller spinning accelerations. The quantities α_{k-1}^* and $\mathbf{u}_{w,k-1}^*$ are the solution of the optimization problem (14) at the previous time step. $\|\cdot\|_{\mathbf{W}_i}$ is the 2-norm weighted by the positive definite weight matrix \mathbf{W}_i . Alternatively, if

the bounds on the propeller accelerations are identified, as in [21], J_3 could be also expressed as a unilateral constraint.

The equality constraint in (14) is the system's dynamics, where we have indicated the inertia matrix as $\mathbf{M} = \begin{bmatrix} m\mathbf{I}_3 & \mathbf{0}_3 \\ \mathbf{0}_3 & \mathbf{J} \end{bmatrix}$, the vector of the gravity and Coriolis terms as $\boldsymbol{\mu} = \begin{bmatrix} -mge_3 \\ -\boldsymbol{\omega} \times \mathbf{J}\boldsymbol{\omega} \end{bmatrix}$, and $\mathbf{J}_R = \begin{bmatrix} \mathbf{R} & \mathbf{0}_3 \\ \mathbf{0}_3 & \mathbf{I}_3 \end{bmatrix}$; the second, unilateral, constraint in (14) expresses the input constraint, where \mathbf{C}, \mathbf{b} are properly defined constant quantities; the last constraint is on the rate of change of α . The maximum rate of change ϵ_α is here defined as symmetric but in the general case they may also be non-symmetric and the analysis still holds.

Please note that J_1 has an equivalent effect to minimizing the norm of the drag moments, as it differs from the input norm by a constant coefficient.

In order to solve problem (14), which is not a QP problem because the first constraint is nonlinear in the optimization variables, we proceed as follows. Consider the following QP problem for a fixed value of α , indicated as $\bar{\alpha}$.

$$\begin{aligned} \min_{\mathbf{u}_w, \ddot{\mathbf{q}}} \quad & J_1 + J_2 + J_3 \\ \text{s.t.} \quad & \mathbf{M}\ddot{\mathbf{q}} = \boldsymbol{\mu} + \mathbf{J}_R \mathbf{F}(\bar{\alpha}) \mathbf{u}_w, \\ & \mathbf{C} \mathbf{u}_w < \mathbf{b} \end{aligned} \quad (15)$$

Problem (15) is now a QP problem as α is not an optimization variable anymore, and, as a consequence, the bilateral constraint is linear in the optimization variables.

At each time step, we solve (15) three times for three different values of $\bar{\alpha} = \{\alpha_{k-1}^* - \epsilon_\alpha, \alpha_{k-1}^*, \alpha_{k-1}^* + \epsilon_\alpha\}$. Hence, at each time step, we pick the solutions α^* and \mathbf{u}_w^* that correspond to the lowest value of the cost function.

Please note that, in principle, the selection of the parameter $\bar{\alpha} \in [\alpha_{k-1}^* - \epsilon_\alpha, \alpha_{k-1}^* + \epsilon_\alpha]$ may be done following different methods. Here we proposed a simple method that allows keeping the value of the tilting angle constant or changing it in the two possible directions accounting for the bound on the variation of α . Other approaches such as an exhaustive search or more efficient sampling algorithms are possibilities, and their assessment is left for future work.

Note that, by tuning the weights \mathbf{W}_i , the control input negotiates between low input effort and low tracking error. We recall that, thanks to its redundancy, the robot is able to follow a certain desired trajectory with different values of the control inputs.

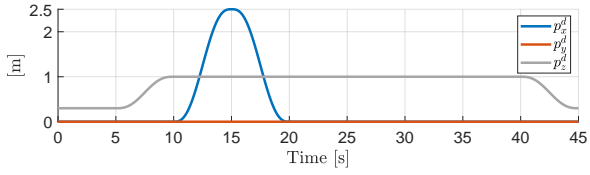
IV. SIMULATIONS

Numerical simulations have been carried out using a URDF description of the OmniMorph and ODE physics engine in Gazebo. The control software has been implemented in Matlab-Simulink. The interface between Matlab and Gazebo is managed by a Gazebo-genom3 plugin². A Simulink s-function embedding qpOases QP solver³ has been used for the optimization problem.

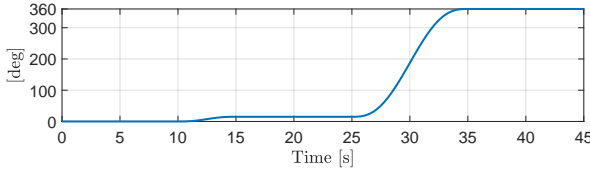
²<https://git.openrobots.org/projects/mrsim-gazebo>

³<https://github.com/coin-or/qpOASES>

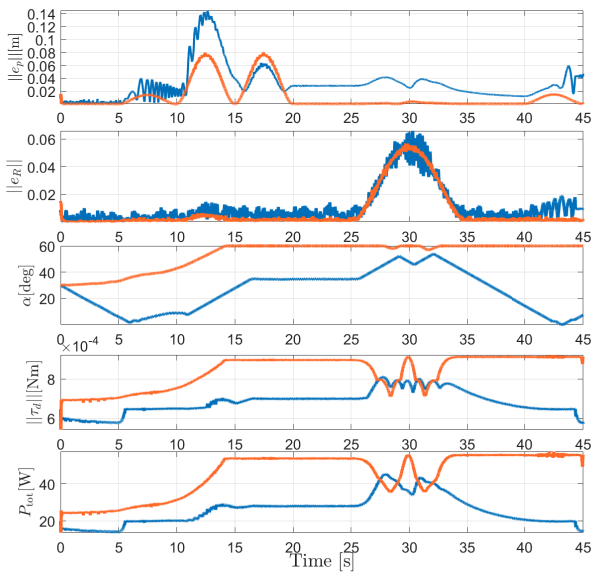
The mass and inertia of the robot are $m = 1.3150 \text{ kg}$



(a) Desired position



(b) Desired attitude expressed as a rotation around x_W



(c) Case A: in orange line; Case B: blue line

and $\mathbf{J} = \text{diag}(1.16 \cdot 10^{-2}, 1.13 \cdot 10^{-2}, 1.13 \cdot 10^{-2}) \text{ Nms}^2$. The other parameters are $\mathbf{K}_{p1} = \text{diag}(60, 60, 60) \text{ s}^{-1}$, $\mathbf{K}_{p2} = \text{diag}(100, 100, 150) \text{ s}^{-2}$, $\mathbf{K}_{\omega 1} = \text{diag}(60, 60, 2) \text{ s}^{-1}$, $\mathbf{K}_{\omega 2} = \text{diag}(300, 300, 20) \text{ s}^{-2}$, $W3 = 10^{-5} \mathbf{I}_8$. The tilting angle α is saturated at 60 deg, a value sufficient to reach the omnidirectionality, as it will be in the real robot.

We show two different simulation scenarios, let us refer to them as Case A and Case B, in which the robot's desired trajectory is the same, but the optimization gains are different. Especially, the trajectory includes moving upwards/downwards, translating with a tilted attitude, and rotating by 360 degrees on the spot—see Figures 3a and 3b. It has been chosen to cover the whole spectrum of the actuation modes: the vertical motion with constant upward orientation is feasible in the underactuated mode, the lateral translations with constant upward orientation require full actuation, and the full 360deg rotation on the spot about a horizontal axis requires omnidirectionality.

What distinguishes the two scenarios is that Case A is

characterized by a lower weight on the input, \mathbf{W}_1 , and a higher weight on the tracking error, \mathbf{W}_2 , than Case B.

The optimization weights for Case A are $\mathbf{W}_1 = 10^{-8} \mathbf{I}_8$ and $\mathbf{W}_2 = \text{diag}(3 \cdot 10^6, 3 \cdot 10^6, 3 \cdot 10^6, 10^3, 10^3, 10^3)$. The optimization weights for Case B are $\mathbf{W}_1 = 10^{-5} \mathbf{I}_8$ and $\mathbf{W}_2 = \text{diag}(3 \cdot 10^4, 3 \cdot 10^4, 3 \cdot 10^4, 1, 1, 1)$.

In Figure 3c, we report a comparison between the results of the two simulation scenarios. One can appreciate as in Case A the robot performs better in terms of tracking (mean square position and attitude errors are, respectively, 0.011 cm and 0.008), at the expenses of a higher motor torque; the tilting angle is increased and kept at the highest value along the task execution. On the contrary, in Case B, the errors are higher (mean square position and attitude errors are, respectively, 0.031 m and 0.011), but the motor torque is, as expected, lower, and the propeller tilting angle is decreased as soon as the robot only moves vertically (as soon as the underactuated mode is enough to perform the desired motion); the efficiency is better in Case B with a total consumed energy of 1151.4 J against 2042.1 J in Case A, which guarantees an increase of the flight time of about 70%.

V. CONCLUSIONS

This work presented the design of the OmniMorph, a novel morphing multirotor that can range between omnidirectionality and underactuation thanks to actively tilting propellers. The design leverages one single servomotor to synchronously tilt all the propellers, thus reducing the mechanical complexity and the additional payload. The dynamics model was presented, and the actuation properties depending on the propeller tilting angles were studied. Hence, a controller was proposed to negotiate between input effort and tracking performance. Simulations in a realistic Gazebo environment were presented.

In the future, experiments on the real prototype will be carried out, and predictive controllers will be tested. Equipping the OmniMorph with physical interaction capabilities in an interesting future direction.

REFERENCES

- [1] A. Ollero, M. Tognon, A. Suarez, D. Lee, and A. Franchi, "Past, Present, and Future of Aerial Robotic Manipulators," *IEEE Transactions on Robotics*, vol. 38, no. 1, pp. 626–645, Feb. 2022, conference Name: IEEE Transactions on Robotics.
- [2] M. Tognon, R. Alami, and B. Siciliano, "Physical Human-Robot Interaction With a Tethered Aerial Vehicle: Application to a Force-Based Human Guiding Problem," *IEEE Transactions on Robotics*, vol. 37, no. 3, pp. 723–734, Jun. 2021, conference Name: IEEE Transactions on Robotics.
- [3] M. Tognon, H. A. T. Chávez, E. Gasparin, Q. Sablé, D. Bicego, A. Mallet, M. Lany, G. Santi, B. Revaz, J. Cortés *et al.*, "A truly-redundant aerial manipulator system with application to push-and-slide inspection in industrial plants," *IEEE Robotics and Automation Letters*, vol. 4, no. 2, pp. 1846–1851, 2019.
- [4] C. Gabellieri, M. Tognon, D. Sanalidro, and A. Franchi, "Equilibria, stability, and sensitivity for the aerial suspended beam robotic system subject to model uncertainty," *arXiv preprint arXiv:2302.07031*, 2023.
- [5] G. Corsini, M. Jacquet, H. Das, A. Afifi, D. Sidobre, and A. Franchi, "Nonlinear model predictive control for human-robot handover with application to the aerial case," in *2022 IEEE/RSJ International Conference on Intelligent Robots and Systems (IROS)*. IEEE, 2022, pp. 7597–7604.

- [6] M. Hamandi, F. Usai, Q. Sablé, N. Staub, M. Tognon, and A. Franchi, "Design of multirotor aerial vehicles: A taxonomy based on input allocation," *The International Journal of Robotics Research*, vol. 40, no. 8-9, pp. 1015–1044, Aug. 2021, publisher: SAGE Publications Ltd STM. [Online]. Available: <https://doi.org/10.1177/02783649211025998>
- [7] M. Hamandi, Q. Sable, M. Tognon, and A. Franchi, "Understanding the omnidirectional capability of a generic multi-rotor aerial vehicle," in *2021 Aerial Robotic Systems Physically Interacting with the Environment (AIRPHARO)*, Oct. 2021, pp. 1–6.
- [8] M. Hamandi, K. Sawant, M. Tognon, and A. Franchi, "Omni-Plus-Seven (O7+): An Omnidirectional Aerial Prototype with a Minimal Number of Unidirectional Thrusters," in *2020 International Conference on Unmanned Aircraft Systems (ICUAS)*, Sep. 2020, pp. 754–761, iSSN: 2575-7296.
- [9] D. Brescianini and R. D'Andrea, "Design, modeling and control of an omni-directional aerial vehicle," in *2016 IEEE International Conference on Robotics and Automation (ICRA)*, May 2016, pp. 3261–3266.
- [10] S. Park, J. Her, J. Kim, and D. Lee, "Design, modeling and control of omni-directional aerial robot," in *2016 IEEE/RSJ International Conference on Intelligent Robots and Systems (IROS)*, Oct. 2016, pp. 1570–1575, iSSN: 2153-0866.
- [11] S. Park, J. Lee, J. Ahn, M. Kim, J. Her, G.-H. Yang, and D. Lee, "ODAR: Aerial Manipulation Platform Enabling Omnidirectional Wrench Generation," *IEEE/ASME Transactions on Mechatronics*, vol. 23, no. 4, pp. 1907–1918, Aug. 2018, conference Name: IEEE/ASME Transactions on Mechatronics.
- [12] M. Tognon and A. Franchi, "Omnidirectional Aerial Vehicles With Unidirectional Thrusters: Theory, Optimal Design, and Control," *IEEE Robotics and Automation Letters*, vol. 3, no. 3, pp. 2277–2282, Jul. 2018, conference Name: IEEE Robotics and Automation Letters.
- [13] M. Ryll, H. H. Bühlhoff, and P. R. Giordano, "A Novel Overactuated Quadrotor Unmanned Aerial Vehicle: Modeling, Control, and Experimental Validation," *IEEE Transactions on Control Systems Technology*, vol. 23, no. 2, pp. 540–556, Mar. 2015, conference Name: IEEE Transactions on Control Systems Technology.
- [14] M. Kamel, S. Verling, O. Elkhatib, C. Sprecher, P. Wulkop, Z. Taylor, R. Siegwart, and I. Giltschenski, "The Voliro Omniorientational Hexacopter: An Agile and Maneuverable Tilttable-Rotor Aerial Vehicle," *IEEE Robotics & Automation Magazine*, vol. 25, no. 4, pp. 34–44, Dec. 2018, conference Name: IEEE Robotics & Automation Magazine.
- [15] M. Allenspach, K. Bodie, M. Brunner, L. Rinsoz, Z. Taylor, M. Kamel, R. Siegwart, and J. Nieto, "Design and optimal control of a tiltrotor micro-aerial vehicle for efficient omnidirectional flight," *The International Journal of Robotics Research*, vol. 39, no. 10-11, pp. 1305–1325, Sep. 2020, publisher: SAGE Publications Ltd STM. [Online]. Available: <https://doi.org/10.1177/0278364920943654>
- [16] M. Ryll, D. Bicego, and A. Franchi, "Modeling and control of FAST-Hex: A fully-actuated by synchronized-tilting hexarotor," in *2016 IEEE/RSJ International Conference on Intelligent Robots and Systems (IROS)*, Oct. 2016, pp. 1689–1694, iSSN: 2153-0866.
- [17] M. Ryll, D. Bicego, M. Giurato, M. Lovera, and A. Franchi, "FAST-Hex—A Morphing Hexarotor: Design, Mechanical Implementation, Control and Experimental Validation," *IEEE/ASME Transactions on Mechatronics*, vol. 27, no. 3, pp. 1244–1255, Jun. 2022, conference Name: IEEE/ASME Transactions on Mechatronics.
- [18] G. Michieletto, M. Ryll, and A. Franchi, "Fundamental actuation properties of multirotors: Force–moment decoupling and fail–safe robustness," *IEEE Transactions on Robotics*, vol. 34, no. 3, pp. 702–715, 2018.
- [19] D. Brescianini and R. D'Andrea, "An omni-directional multirotor vehicle," *Mechatronics*, vol. 55, pp. 76–93, Nov. 2018. [Online]. Available: <https://www.sciencedirect.com/science/article/pii/S0957415818301314>
- [20] T. Lee, M. Leok, and N. H. McClamroch, "Geometric tracking control of a quadrotor UAV on SE(3)," in *49th IEEE conference on decision and control*. IEEE, 2010, pp. 5420–5425.
- [21] D. Bicego, J. Mazzetto, R. Carli, M. Farina, and A. Franchi, "Nonlinear model predictive control with enhanced actuator model for multirotor aerial vehicles with generic designs," *Journal of Intelligent & Robotic Systems*, vol. 100, pp. 1213–1247, 2020.